

**Superconductors in realistic geometries: Geometric edge barrier versus pinning**

Ernst Helmut Brandt

*Max-Planck-Institut für Metallforschung, D-70506 Stuttgart, Germany*

(February 1, 2008)

The magnetic response of type-II superconductors can be irreversible due to two different reasons: vortex pinning and barriers for flux penetration. Even without bulk pinning and in absence of a microscopic Bean-Livingston surface barrier for vortex penetration, superconductors of nonellipsoidal shape can exhibit a large geometric barrier for flux penetration. This edge barrier and the resulting irreversible magnetization loops and flux-density profiles are computed from continuum electrodynamics for superconductor strips and disks with constant thickness, both without and with bulk pinning. Expressions for the field of first flux entry  $H_{\text{en}}$  and for the reversibility field  $H_{\text{rev}}$  above which the pin-free magnetization becomes reversible are given. Both fields are proportional to the lower critical field  $H_{c1}$  and else depend only on the specimen shape. These realistic results are compared with the reversible magnetic behavior of ideal superconductor ellipsoids.

PACS numbers: **74.60.Ec, 74.60.Ge, 74.55.+h****I. INTRODUCTION**

The irreversible magnetic behavior of type-II superconductors usually is caused by pinning of the vortices at inhomogeneities in the material [1]. However, similar hysteresis effects were also observed [2] in type-I superconductors, which do not contain flux lines, and in type-II superconductors with negligible pinning. In these two cases the magnetic irreversibility is caused by a geometric (specimen-shape dependent) barrier which delays the penetration of magnetic flux but not its exit. In this respect the *macroscopic* geometric barrier behaves similar as the *microscopic* Bean-Livingston barrier [3] for straight vortices penetrating at a parallel surface. In both cases the magnetic irreversibility is caused by the asymmetry between flux penetration and exit. The geometric irreversibility is most pronounced for thin films of constant thickness in a perpendicular field. It is absent only when the superconductor is of exactly ellipsoidal shape or is tapered like a wedge with a sharp edge where flux can penetrate easily due to the large local enhancement of the external magnetic field at this edge in a diamagnetic material.

Ellipsoids are a particular case. In superconducting ellipsoids the inward directed driving force exerted on the vortex ends by the surface screening currents is exactly compensated by the vortex line tension [4]. An isolated vortex line is thus in an indifferent equilibrium at any distance from the specimen center. The repulsive vortex interaction therefore yields a uniform flux density and the magnetization is reversible. However, in specimens with constant thickness (i.e. with rectangular cross-section) this line tension opposes the penetration of flux lines at the four corner lines, thus causing an edge barrier; but as soon as two penetrating vortex segments join at the equator they contract and are driven to the specimen center by the surface currents, see Figs. 1 and 2. As

opposed to this, when the specimen profile is tapered and has a sharp edge, the driving force of the screening currents even in very weak applied field exceeds the restoring force of the line tension such that there is no edge barrier. The resulting absence of hysteresis in wedge-shaped samples was clearly shown by Morozov et al. [5].

For thin superconductor strips with an edge barrier an elegant analytical theory of the field and current profiles has been presented by Zeldov et al. [6], using the theory of complex functions, see also the calculations [7,8]. With increasing applied field  $H_a$ , the magnetic flux does not penetrate until an entry field  $H_{\text{en}}$  is reached; at  $H_a = H_{\text{en}}$  the flux immediately jumps to the center, from where it gradually fills the entire strip or disk. This behavior in increasing  $H_a$  is similar to that of thin films with artificially enhanced pinning near the edges [7,9], but in decreasing  $H_a$  the behavior is different: In films with enhanced edge pinning (critical current density  $J_c^{\text{edge}}$ ) the current density  $J$  at the edge immediately jumps from  $+J_c^{\text{edge}}$  to  $-J_c^{\text{edge}}$  when the ramp rate reverses its sign, while in pin-free films with geometric barrier the current density at the edge first stays constant or even increases and then gradually decreases and reaches zero at  $H_a = 0$ . For pin-free thin strips the entry field  $H_{\text{en}}$  was estimated in Refs. [6,10,11].

The outline of the present work is as follows. Section 2 discusses the reversible magnetic behavior of pin-free superconductor ellipsoids. The effective demagnetization factor of long strips (or slabs) and circular disks (or cylinders) with rectangular cross section  $2a \times 2b$  is given in Sec. 3. In Sec. 4 appropriate continuum equations and algorithms are presented that allow to compute the magnetic irreversibility caused by pinning and/or by the geometric barrier in type-II superconductors of arbitrary shape, in particular of strips and disks with finite thickness. Results for thick long strips and disks or cylinders with arbitrary aspect ratio  $b/a$  are given in Sec. 5 for

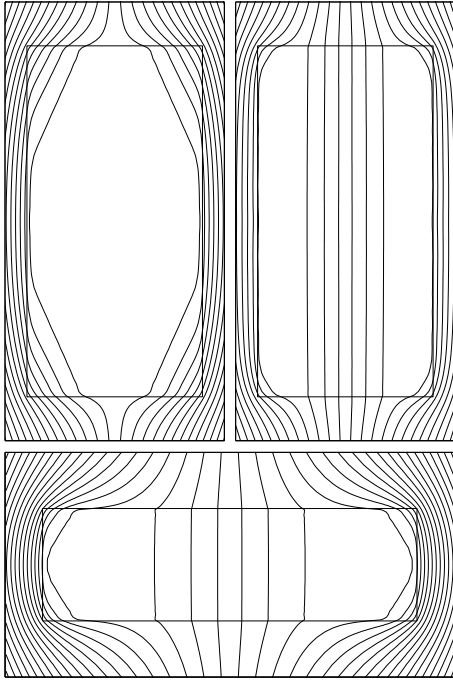


FIG. 1. Field lines of the induction  $\mathbf{B}(x, y)$  in strips with aspect ratio  $b/a = 2$  (top) and  $b/a = 0.3$  (bottom) in perpendicular magnetic field  $H_a$ . Top left:  $H_a/H_{c1} = 0.66$ , in increasing field shortly before the entry field  $H_{en}/H_{c1} = 0.665$ . Top right:  $H_a/H_{c1} = 0.5$ , decreasing field. Bottom:  $H_a/H_{c1} = 0.34$  in increasing field just above  $H_{en}/H_{c1} = 0.32$ . Note the nearly straight field lines in the corners indicating the tension of the flux lines. The field lines of cylinders look very similar.

pin-free superconductors and in Sec. 6 for superconductors with arbitrary bulk pinning. In particular, explicit expressions are given for the field of first flux entry  $H_{en}$  and for the reversibility field  $H_{rev}$  above which the magnetization curve is reversible and coincides with that of an ellipsoid.

## II. ELLIPSOIDS

First consider the known magnetization of ideal ellipsoids. If the superconductor is homogeneous and isotropic, the magnetization curves of ellipsoids  $M(H_a; N)$  are *reversible* and may be characterized by a demagnetizing factor  $N$ . If  $H_a$  is along one of the three principal axes of the ellipsoid then  $N$  is a scalar with  $0 \leq N \leq 1$ . One has  $N = 0$  for long specimens in parallel field,  $N = 1$  for thin films in perpendicular field,  $N = 1/2$  for transverse circular cylinders, and  $N = 1/3$  for spheres. For general ellipsoids with semi-axes  $a, b, c$  along the cartesian axes  $x, y, z$ , the three demagnetizing factors along the principal axes satisfy  $N_x + N_y + N_z = 1$ . For rotational ellipsoids with  $a = b$  one has  $N_x = N_y = (1 - N_z)/2$  where for cigars

with  $a = b < c$  and for disks with  $a = b > c$  with eccentricity  $e = |1 - c^2/a^2|^{1/2}$  one obtains [12]

$$\begin{aligned} N_z &= \frac{1 - e^2}{e^3} (\operatorname{atanh} e - e), \quad (\text{cigar}), \\ N_z &= \frac{1 - e^2}{e^3} (e - \operatorname{atanh} e), \quad (\text{disk}). \end{aligned} \quad (1)$$

For thin ellipsoidal disks with  $a \geq b \gg c$  one has [13]

$$N_z = 1 - \frac{c}{b} E(k), \quad (2)$$

where  $E(k)$  is the complete elliptic integral of the second kind with  $k^2 = 1 - b^2/a^2$ .

When the magnetization curve in parallel field is known,  $M(H_a; 0) = B/\mu_0 - H_a$  where  $B$  is the flux density inside the ellipsoid, then the homogeneous magnetization of the general ellipsoid,  $M(H_a; N)$ , follows from the implicit equation

$$H_i = H_a - N M(H_i; 0). \quad (3)$$

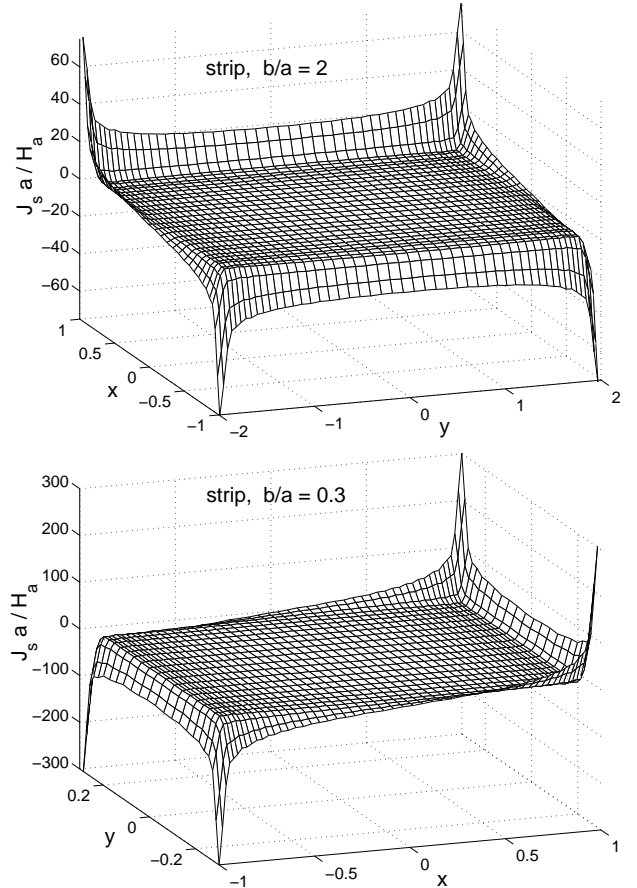


FIG. 2. 3D plots of the screening current density  $J_s(x, y)$ , Eq. (11), in superconductor strips with  $b/a = 2$  (top) and  $b/a = 0.3$  (bottom) as in Fig. 1. Shown is the limit of small applied field  $H_a \ll H_{c1}$  before magnetic flux has penetrated. For better presentation the depicted  $J_s(x, y)$  is smeared over a few grid cells.

Solving Eq. (3) for the effective internal field  $H_i$ , one obtains  $M = M(H_a; N) = M(H_i; 0)$ . In particular, for the Meissner state ( $B \equiv 0$ ) one finds  $M(H_a; 0) = -H_a$  and

$$M(H_a; N) = -\frac{H_a}{1-N} \quad \text{for } |H_a| \leq (1-N)H_{c1}. \quad (4)$$

At the lower critical field  $H_{c1}$  one has  $H_i = H_{c1}$ ,  $H_a = H'_{c1} = (1-N)H_{c1}$ ,  $B = 0$ , and  $M = -H_{c1}$ . Near the upper critical field  $H_{c2}$  one has an approximately linear  $M(H_a; 0) = \gamma(H_a - H_{c2}) < 0$  with  $\gamma > 0$ , yielding

$$M(H_a; N) = \frac{\gamma}{1+\gamma N}(H_a - H_{c2}) \quad \text{for } H_a \approx H_{c2}. \quad (5)$$

Thus, if the slope  $\gamma \ll 1$  is small (and in general, if  $|M/H_a| \ll 1$  is small), demagnetization effects may be disregarded and one has  $M(H_a; N) \approx M(H_a; 0)$ .

The ideal magnetization curve of type-II superconductors with  $N = 0$ ,  $M(H_a; 0)$  or  $B(H_a; 0)/\mu_0 = H_a + M(H_a; 0)$ , may be calculated from Ginzburg-Landau (GL) theory [14], but to illustrate the geometric barrier any other model curve may be used provided  $M(H_a; 0) = -M(-H_a; 0)$  has a vertical slope at  $H_a = H_{c1}$  and decreases monotonically in size for  $H_a > H_{c1}$ . Below for simplicity I shall assume  $H_{c1} \ll H_{c2}$  (i.e. large GL parameter  $\kappa \gg 1$ ) and  $H_a \ll H_{c2}$ . In this case one may use the model  $M(H_a; 0) = -H_a$  for  $|H_a| \leq H_{c1}$  and

$$M(H_a; 0) = (H_a/|H_a|)(|H_a|^3 - H_{c1}^3)^{1/3} - H_a \quad (6)$$

for  $|H_a| > H_{c1}$ , which well approximates the pin-free GL magnetization [14].

### III. THICK STRIPS AND DISKS IN THE MEISSNER STATE

In nonellipsoidal superconductors the induction  $\mathbf{B}(\mathbf{r})$  in general is not homogeneous, and so the concept of a demagnetizing factor does not work. However, when the magnetic moment  $\mathbf{m} = \frac{1}{2} \int \mathbf{r} \times \mathbf{J}(\mathbf{r}) d^3r$  is directed along  $H_a$ , one may define an *effective demagnetizing factor*  $N$  which in the Meissner state ( $B \equiv 0$ ) yields the same slope  $M/H_a = -1/(1-N)$ , Eq. (2), as an ellipsoid with this  $N$ . Here the definition  $M = m/V$  with  $m = \mathbf{m}H_a/H_a$  and specimen volume  $V$  is used. In particular, for long strips or slabs and circular disks or cylinders with rectangular cross-section  $2a \times 2b$  in a perpendicular or axial magnetic field along the thickness  $2b$ , approximate expressions for the slopes  $M/H_a = m/(VH_a)$  are given in Refs. [15,16]. Using this and defining  $q \equiv (|M/H_a| - 1)(b/a)$ , one obtains the effective  $N$  for any aspect ratio  $b/a$  in the form

$$N = 1 - 1/(1 + qa/b),$$

$$q_{\text{strip}} = \frac{\pi}{4} + 0.64 \tanh \left[ 0.64 \frac{b}{a} \ln \left( 1.7 + 1.2 \frac{a}{b} \right) \right],$$

$$q_{\text{disk}} = \frac{4}{3\pi} + \frac{2}{3\pi} \tanh \left[ 1.27 \frac{b}{a} \ln \left( 1 + \frac{a}{b} \right) \right]. \quad (7)$$

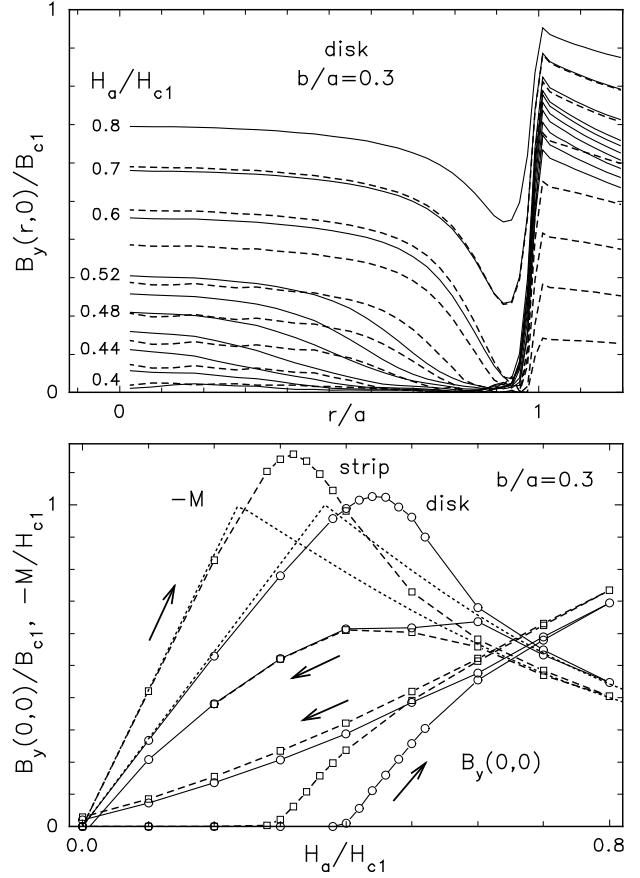


FIG. 3. Top: The axial magnetic induction  $B_y(r, y)$  in the midplane  $y = 0$  of a pin-free superconductor disk with aspect ratio  $b/a = 0.3$  in increasing field (solid lines) and then decreasing field (dashed lines), plotted at  $H_a/H_{c1} = 0.4, 0.42, \dots, 0.5, 0.52, 0.6, 0.7, 0.8, 0.7, 0.6, \dots, 0.1, 0$ . Bottom: The induction  $B_y(0, 0)$  in the center of the same disk (solid line) and of a strip (dashed line), both with  $b/a = 0.3$ . The symbols mark the field values at which the profiles are taken. Also shown is the magnetization loop for the same disk and strip and the corresponding reversible magnetization (dotted lines).

In the limits  $b \ll a$  and  $b \gg a$ , these formulae are exact, and for general  $b/a$  the relative error is  $< 1\%$ . For  $a = b$  (square cross-section) they yield for the strip  $N = 0.538$  (while  $N = 1/2$  for a circular cylinder in perpendicular field) and for the short cylinder  $N = 0.365$  (while  $N = 1/3$  for the sphere).

### IV. COMPUTATIONAL METHOD

To obtain the full, irreversible magnetization curves  $M(H_a)$  of nonellipsoidal superconductors one has to resort to numerics. Appropriate continuum equations and algorithms have been proposed recently by Labusch and Doyle [17] and by the author [18], based on the Maxwell

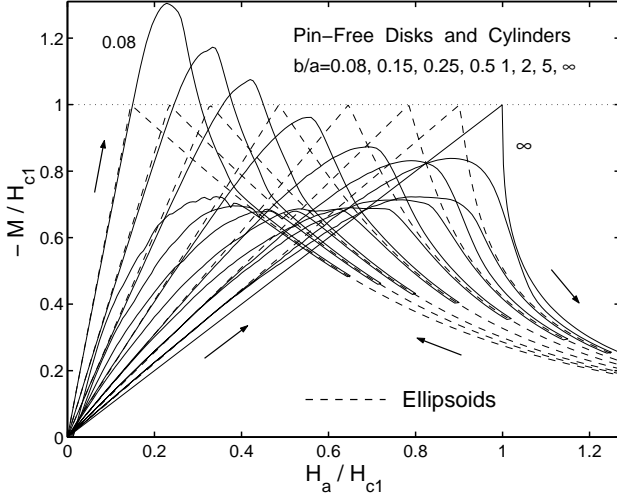


FIG. 4. The irreversible magnetization curves  $-M(H_a)$  of pin-free circular disks and cylinders with aspect ratios  $b/a = 0.08, 0.15, 0.25, 0.5, 1, 2, 5$ , and  $\infty$  in an axial field (solid lines). Here the irreversibility is due only to a geometric edge barrier for flux penetration. The reversible magnetization curves of the corresponding ellipsoids defined by Eqs. (3,6,7) are shown as dashed lines.

equations and on constitutive laws which describe flux flow and pinning or thermal depinning, and the equilibrium magnetization in absence of pinning,  $M(H_a; 0)$ . For arbitrary specimen shape these two methods proceed as follows.

While method [17] considers a magnetic charge density on the specimen surface which causes an effective field  $\mathbf{H}_i(\mathbf{r})$  inside the superconductor, our method [18] couples the arbitrarily shaped superconductor to the external field  $\mathbf{B}(\mathbf{r}, t)$  via surface screening currents: In a first step the vector potential  $\mathbf{A}(\mathbf{r}, t)$  is calculated for given current density  $\mathbf{J}$ ; then this linear relation (a matrix) is inverted to obtain  $\mathbf{J}$  for given  $\mathbf{A}$  and given  $\mathbf{H}_a$ ; next the induction law is used to obtain the electric field [in our symmetric geometry one has  $\mathbf{E}(\mathbf{J}, \mathbf{B}) = -\partial\mathbf{A}/\partial t$ ], and finally the constitutive law  $\mathbf{E} = \mathbf{E}(\mathbf{J}, \mathbf{B})$  is used to eliminate  $\mathbf{A}$  and  $\mathbf{E}$  and obtain one single integral equation for  $\mathbf{J}(\mathbf{r}, t)$  as a function of  $\mathbf{H}_a(t)$ , without having to compute  $\mathbf{B}(\mathbf{r}, t)$  outside the specimen. This method in general is fast and elegant; but so far the algorithm is restricted to aspect ratios  $0.03 \leq b/a \leq 30$ , and to a number of grid points not exceeding 1400 (on a Personal Computer). Improved accuracy is expected by combining the methods [17] (working best for small  $b/a$ ) and [18]. Here I shall use the method [18] and simplify it to the two-dimensional (2D) geometry of thick strips and disks.

In the 2D geometry of thick strips [15] or short cylinders [16] in an applied magnetic field  $\mathbf{B}_a = \mu_0 \mathbf{H}_a = \nabla \times \mathbf{A}_a$  along  $y$ , one writes  $\mathbf{r} = (x, y)$  or  $\mathbf{r} = (\rho, y)$  (in cylindrical coordinates  $\rho, \varphi, y$ ). For a homogeneous applied field the applied vector potential in these two geometries reads  $A_a = -xB_a$  or  $A_a = -\rho B_a/2$ . The current

density  $\mathbf{J}(\mathbf{r}, t)$ , electric field  $\mathbf{E}(\mathbf{r}, t)$ , and vector potential  $\mathbf{A}(\mathbf{r}, t)$  now have only one component oriented along  $z$  or  $\varphi$  and denoted by  $J, E, A$ . The method [15,16,18] describes the superconductor by its current density  $J(\mathbf{r}, t)$ , from which the magnetic field  $\mathbf{B}(x, y, t) = (B_x, B_y)$  or  $\mathbf{B}(\rho, y, t) = (B_\rho, B_y)$ , the magnetic moment  $m(t)$  (along  $y$ ), and the electric field  $E(\mathbf{r}, t) = E(J, \mathbf{B}, \mathbf{r}')$  follow directly or via the constitutive law  $E = E(J, \mathbf{B})$ . For high inductions  $B \gg \mu_0 H_{c1}$  one has  $\mathbf{B} = \mu_0 \mathbf{H}$  everywhere and  $J = -\nabla^2(A - A_a)$ . The current density  $J$  is then obtained by time-integrating the following equation of motion,

$$\dot{J}(\mathbf{r}, t) = \int_V d^2r' K(\mathbf{r}, \mathbf{r}') [E(J, \mathbf{B}) + \dot{A}_a(\mathbf{r}', t)]. \quad (8)$$

Here  $K(\mathbf{r}, \mathbf{r}') = Q(\mathbf{r}, \mathbf{r}')^{-1}$  is an inverse integral kernel obtained by inverting a matrix, see [15,16] for details. The kernels  $Q$  and  $K$  apply to the appropriate geometry and relate  $J$  to the current-caused vector potential  $A - A_a$  in the (here trivial) gauge  $\nabla \cdot \mathbf{A} = 0$  via integrals over the specimen volume  $V$ ,

$$A(\mathbf{r}) = - \int_V d^2r' Q(\mathbf{r}, \mathbf{r}') J(\mathbf{r}') + A_a(\mathbf{r}), \quad (9)$$

$$J(\mathbf{r}) = - \int_V d^2r' K(\mathbf{r}, \mathbf{r}') [A(\mathbf{r}') - A_a(\mathbf{r}')]. \quad (10)$$

The Laplacian kernel  $Q$  is universal, e.g.,  $Q(\mathbf{r}, \mathbf{r}') = -(\mu_0/2\pi) \ln|\mathbf{r} - \mathbf{r}'|$  for long strips with arbitrary cross section, but the inverse kernel  $K$  depends on the shape of the specimen cross section. Putting  $A(\mathbf{r}') = 0$  in Eq. (10) (Meissner state) one sees that

$$J_s(\mathbf{r}) = \int_V d^2r' K(\mathbf{r}, \mathbf{r}') A_a(\mathbf{r}') \quad (11)$$

is the surface screening current caused by the applied field. In particular, one has  $J_s(\mathbf{r}) = 0$  inside the superconductor. In our method  $J_s$  automatically is restricted to the layer of grid points nearest to the surface, see Fig. 2.

If one is interested also in low inductions one has to generalize Eq. (8) to general reversible magnetization  $\mathbf{H} = \mathbf{H}(\mathbf{B})$ . This is achieved by replacing in the constitutive law  $\mathbf{E}(\mathbf{J}, \mathbf{B})$  the genuine current density  $\mathbf{J} = \mu_0^{-1} \nabla \times \mathbf{B}$  by the effective current density  $\mathbf{J}_H = \nabla \times \mathbf{H}$  which drives the vortices and thereby generates an electric field  $\mathbf{E}$ . That  $\mathbf{J}_H = \nabla \times \mathbf{H}(\mathbf{B}, \mathbf{r})$  enters the Lorentz force is rigorously proven by Labusch [17]. Within the London theory this important relation may also be concluded from the facts that the force on a vortex is determined by the *local* current density at the vortex center, while the energy density  $F$  of the vortex lattice is determined by the magnetic field at the vortex centers. Thus,  $\mathbf{J}_H = \nabla \times (\partial F / \partial \mathbf{B})$  is the average of the current densities at the vortex centers, which in general is different from

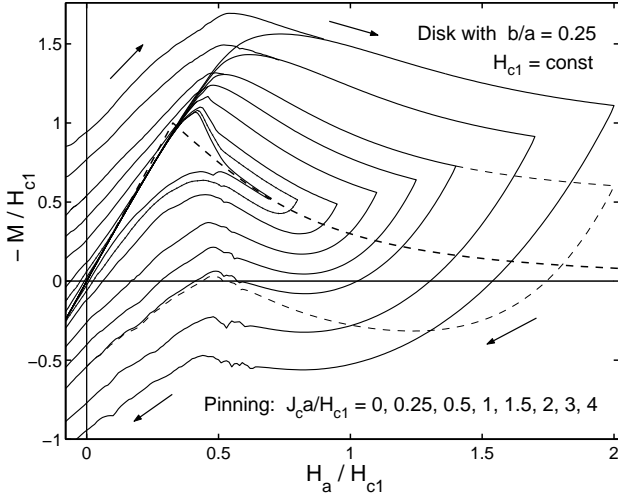


FIG. 5. The magnetization curves  $M(-H_a) = -M(H_a)$  of a thick disk with aspect ratio  $b/a = 0.25$  and constant  $H_{c1}$  for various pinning strengths,  $J_c = 0, 0.25, 0.5, 1, 1.5, 2, 3, 4$  in units  $H_{c1}/a$ , and various sweep amplitudes. Bean model. The inner loop belongs to the pin-free disk ( $J_c = 0$ ), the outer loop to strongest pinning. The reversible magnetization curve of the corresponding ellipsoid is shown as a dashed curve.

the current density  $\mathbf{J} = \mu_0^{-1} \nabla \times \mathbf{B}$  averaged over the vortex cells. In our 2D geometry one thus has to replace in Eq. (8)

$$E[\mathbf{J}(\mathbf{r}'), \mathbf{B}(\mathbf{r}')] \rightarrow E[\mathbf{J}_H(\mathbf{r}'), \mathbf{B}(\mathbf{r}')], \quad (12)$$

where  $J_H = \partial H_y / \partial x - \partial H_x / \partial y$  depends on the reversible material law  $H(B) = \partial F / \partial B$  with  $H_x = H(B)B_x/B$ ,  $H_y = H(B)B_y/B$ , and  $B = (B_x^2 + B_y^2)^{1/2}$ .

The boundary condition on  $\mathbf{H}(\mathbf{r})$  is simply that one has  $\mathbf{H} = \mathbf{B}/\mu_0$  at the surface (and in the vacuum outside the superconductor, which does not enter our calculation). This boundary condition may be forced by an appropriate space-dependent material law  $\mathbf{H} = \mathbf{H}(\mathbf{B}, \mathbf{r})$ , which outside and at the surface of the superconductor is trivially  $\mathbf{H} = \mathbf{B}/\mu_0$ . The specimen shape thus enters in two places: via the integral kernel  $K(\mathbf{r}, \mathbf{r}')$  and via the material law  $\mathbf{H} = \mathbf{H}(\mathbf{B}, \mathbf{r})$ .

To compute the induction  $\mathbf{B}(\mathbf{r})$  entering  $\mathbf{H}(\mathbf{B})$ , for maximum accuracy one should not use the derivative  $\mathbf{B} = \nabla \times \mathbf{A}$  but the Biot-Savart integral

$$\mathbf{B}(\mathbf{r}) = \int_V d^2 r' \mathbf{L}(\mathbf{r}, \mathbf{r}') J(r') + \mathbf{B}_a(\mathbf{r}), \quad (13)$$

with appropriate kernel  $\mathbf{L}(\mathbf{r}, \mathbf{r}')$ . The accuracy of the method then depends mainly on the algorithm used to compute the derivative  $\mathbf{J}_H = \nabla \times \mathbf{H}$ . A useful trick is to compute  $\mathbf{J}_H$  as  $\mathbf{J}_H = \mathbf{J} + \nabla \times (\mathbf{H} - \mathbf{B}/\mu_0)$  where  $\mathbf{H} - \mathbf{B}/\mu_0$  is typically small and vanishes at the surface.

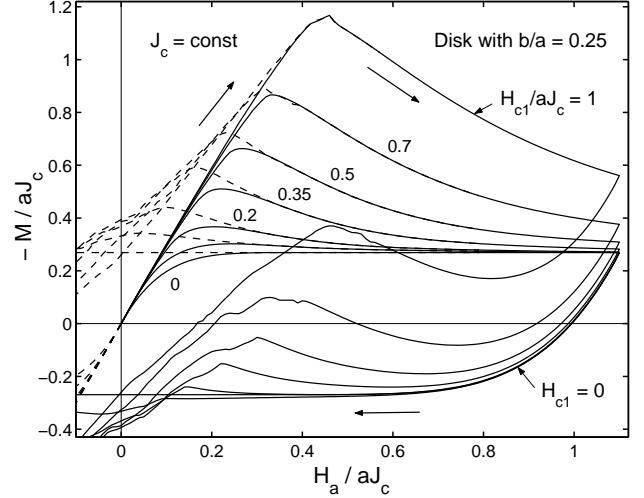


FIG. 6. Magnetization curves of a disk as in Fig. 5 but with  $J_c = \text{const.}$  and for various lower critical fields  $H_{c1} = 0, 0.2, 0.35, 0.5, 0.7, 1$  in units  $aJ_c$ . Bean model.

For the following computations I use simple models for the constitutive laws of an isotropic homogeneous type-II superconductor without Hall effect, though our method [18] is more general. With Eq. (6) and  $H = B/\mu_0 - M$  one has

$$H(B) = \mu_0^{-1} [B_{c1}^3 + B^3]^{1/3}. \quad (14)$$

with  $B_{c1} = \mu_0 H_{c1}$ . A simple  $B$ -dependent current-voltage law which describes pinning, thermal depinning, and flux flow is  $\mathbf{E}(\mathbf{J}, \mathbf{B}) = \rho(J, B)\mathbf{J}$  with

$$\rho(J, B) = \rho_0 B \frac{(J/J_c)^\sigma}{1 + (J/J_c)^\sigma}. \quad (15)$$

This model has the correct limits  $\rho \propto J^\sigma$  ( $J \ll J_c$ , flux creep) and  $\rho = \rho_0 B = \rho_{FF}$  ( $J \gg J_c$ , flux flow,  $\rho_0 = \text{const.}$ ), and for large creep exponent  $\sigma \gg 1$  it reduces to the Bean critical state model. In general the critical current density  $J_c = J_c(B)$  and the creep exponent  $\sigma(B) \geq 0$  will depend on  $B$ . For pin-free superconductors ( $J_c \rightarrow 0$ ) this expression describes usual flux flow, i.e., viscous motion of vortices,  $\mathbf{E} = \rho_{FF}(B)\mathbf{J}$ , with flux-flow resistivity  $\rho_{FF} \propto B$  as it should be.

## V. PIN-FREE SUPERCONDUCTORS

The penetration and exit of flux computed from Eqs. (8-15) is visualized in Figs. 1 – 3 for isotropic strips and disks without volume pinning, using a flux-flow resistivity  $\rho_{FF} = \rho_0 B(\mathbf{r})$  with  $\rho_0 = 140$  (strip) or  $\rho_0 = 70$  (disk) in units where  $H_{c1} = a = \mu_0 = |dH_a/dt| = 1$ . Figure 1 shows the field lines of  $\mathbf{B}(x, y)$  in two pin-free strips with aspect ratios  $b/a = 2$  and  $b/a = 0.3$ ; Fig. 2 shows the surface screening currents in the same strips before flux has penetrated; and Fig. 3 plots some induction profiles in a strip and some hysteresis loops of the magnetization

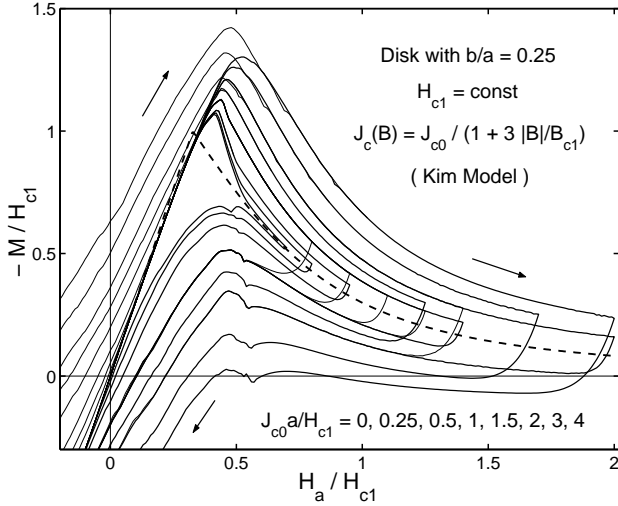


FIG. 7. Magnetization curves of the same disk as in Fig. 5 but for the Kim model,  $J_c(B) = J_{c0}/(1 + 3|B|/B_{c1})$  for various pinning strengths  $J_{c0} = 0, 0.25, 0.5, 1, 1.5, 2, 3, 4$  in units  $H_{c1}/a$ . Presentation as in Fig. 5.

and of the induction in the center of a strip and disk.

The profiles of the induction  $B_y(r, y)$  taken along the midplane  $y = 0$  of the thick disk in Fig. 3 have a pronounced minimum near the edge  $r = a$ , which is the region where strong screening currents flow. Away from the edges, the current density  $\mathbf{J} = \nabla \times \mathbf{B}/\mu_0$  is nearly zero; note the parallel field lines in Fig. 1. The quantity  $\mathbf{J}_H = \nabla \times \mathbf{H}(\mathbf{B})$  which enters the Lorentz force density  $\mathbf{J}_H \times \mathbf{B}$ , is even exactly zero since we assume absence of pinning and the viscous drag force is small. Our finite flux-flow parameter  $\rho_0$  and finite ramp rate  $dH_a/dt = \pm 1$  mean a dragging force which, similar to pinning, causes a weak hysteresis and a small remanent flux at  $H_a = 0$ ; this artefact is reduced by choosing a larger resistivity or a slower ramp rate.

In Fig. 3 the induction  $B_0 = B_y(0, 0)$  in the specimen center performs a hysteresis loop very similar to the magnetization loops  $M(H_a)$  shown in Figs. 3 and 4. Both loops are symmetric,  $M(-H_a) = -M(H_a)$  and  $B_0(-H_a) = -B_0(H_a)$ . The maximum of  $M(H_a)$  defines a field of first flux entry  $H_{en}$ , which closely coincides with the field  $H'_{en}$  at which  $B_y(0, 0)$  starts to appear. The computed entry fields are well fitted by

$$\begin{aligned} H_{en}^{\text{strip}}/H_{c1} &= \tanh \sqrt{0.36b/a}, \\ H_{en}^{\text{disk}}/H_{c1} &= \tanh \sqrt{0.67b/a}. \end{aligned} \quad (16)$$

These formulae are good approximations for all aspect ratios  $0 < b/a < \infty$ , see also the estimates of  $H_{en} \approx \sqrt{b/a}$  for thin strips in Refs. [6,10].

The virgin curve of the irreversible  $M(H_a)$  of strips and disks at small  $H_a$  coincides with the ideal Meissner straight line  $M = -H_a/(1 - N)$  of the corresponding ellipsoid, Eqs. (4,7). When the increasing  $H_a$  approaches  $H_{en}$ , flux starts to penetrate into the corners in form of

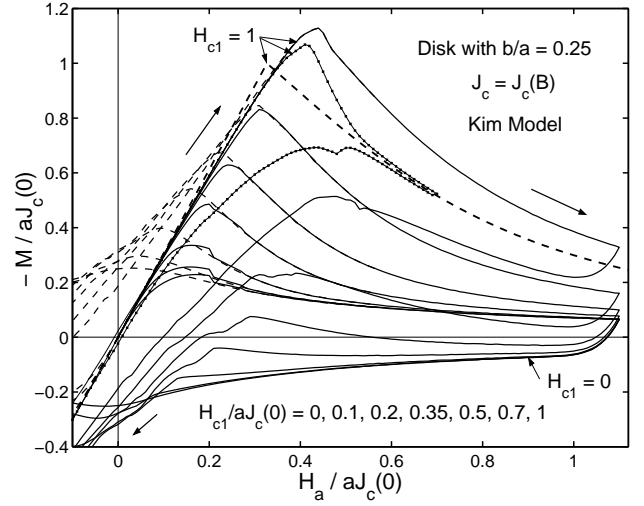


FIG. 8. Magnetization curves as in Fig. 6 but for the Kim model  $J_c(B) = J_{c0}/(1 + 3|B|/aJ_{c0})$  with  $J_{c0} = \text{const.}$  for various  $H_{c1} = 0, 0.2, 0.35, 0.5, 0.7, 1$  in units  $aJ_{c0}$ . Also depicted are the pin-free magnetization (line with dots;  $M$  and  $H_a$  here are in units  $H_{c1}$  since  $J_{c0} = 0$ ) and the irreversible magnetization of the corresponding ellipsoid.

almost straight flux lines (Fig. 1) and thus  $|M(H_a)|$  falls below the Meissner line. At  $H_a = H_{en}$  flux penetrates and jumps to the center, and  $|M(H_a)|$  starts to decrease. In decreasing  $H_a$ , this barrier is absent. As soon as flux exit starts, all our calculated  $M(H_a)$  exhibit strong “numerical noise”, which reflects the instability of this state. Similar but weaker noise occurs at the onset of flux penetration.

As can be seen in Fig. 4, above some field  $H_{rev}$ , the magnetization curve  $M(H_a)$  becomes reversible and exactly coincides with the curve of the ellipsoid defined by Eqs. (3, 6, 7) (in the quasistatic limit with  $\rho_0^{-1}dH_a/dt \rightarrow 0$ ). The irreversibility field  $H_{rev}$  is difficult to compute since it slightly depends on the choices of the flux-flow parameter  $\rho_0$  (or ramp rate) and of the numerical grid, and also on the model for  $M(H_a; 0)$ . In the interval  $0.08 \leq b/a \leq 5$  we find with relative error of 3%,

$$\begin{aligned} H_{rev}^{\text{strip}}/H_{c1} &= 0.65 + 0.12 \ln(b/a), \\ H_{rev}^{\text{disk}}/H_{c1} &= 0.75 + 0.15 \ln(b/a). \end{aligned} \quad (17)$$

This fit obviously does not apply to very small  $b/a \ll 1$  (since  $H_{rev}$  should exceed  $H_{en} > 0$ ) nor to very large  $b/a \gg 1$  (where  $H_{rev}$  should be close to  $H_{c1}$ ). The limiting value of  $H_{rev}$  for thin films with  $b \ll a$  is thus not yet known.

Remarkably, the irreversible magnetization curves  $M(H_a)$  of pin-free strips and disks fall on top of each other if the strip is chosen twice as thick as the disk,  $(b/a)_{\text{strip}} \approx 2(b/a)_{\text{disk}}$ . This striking coincidence holds for all aspect ratios  $0 < b/a < \infty$  and can be seen from

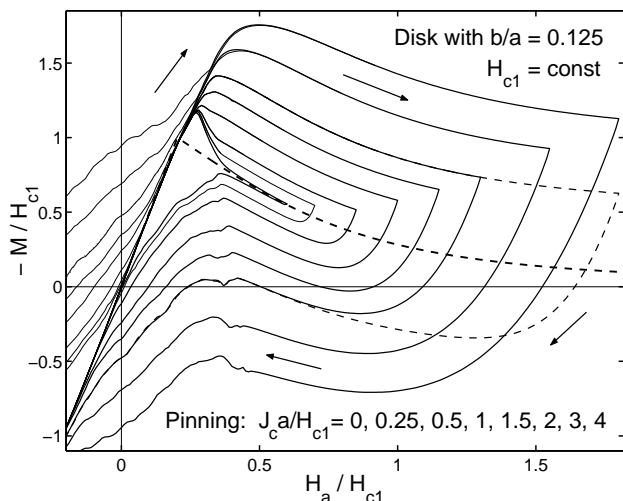


FIG. 9. Same magnetization curves as in Fig. 5 but for a thinner disk with aspect ratio  $b/a = 0.125$  for various degrees of pinning and constant  $H_{c1}$ .

each of Eqs. (7,16,17): The effective  $N$  [or virgin slope  $1/(1-N)$ ], the entry field  $H_{en}$ , and the reversibility field  $H_{rev}$  are nearly equal for strips and disks with half thickness, or for slabs and cylinders with half length.

Another interesting feature of the pin-free magnetization loops is that the maximum of  $|M(H_a)|$  exceeds the maximum of the reversible curve (equal to  $H_{c1}$ ) when  $b/a \leq 0.8$  for strips and  $b/a \leq 0.4$  for disks, but at larger  $b/a$  it falls below  $H_{c1}$ . The maximum magnetization may be estimated from the slope of the virgin curve  $1/(1-N)$ , Eq. (7), and from the field of first flux entry, Eq. (16).

The formulae (7,16,17) are derived essentially from first principles, with no assumptions but the geometry and finite  $H_{c1}$ . They should be used to interpret experiments on superconductors with no or very weak vortex pinning. At present it is not clear how the presence of a microscopic Bean-Livingston barrier may modify these continuum theoretical results.

## VI. SUPERCONDUCTORS WITH PINNING

Figures 5-8 show how the irreversible magnetization loops of disks with  $b/a = 0.25$  (and in Fig. 9 for a thinner disk with  $b/a = 0.125$ ) are modified when volume pinning is switched on. In Figs. 5, 6, and 9, pinning is described by the Bean model with constant critical current density  $J_c$ , while in Figs. 7 and 8 the Kim model is used with an induction-dependent  $J_c(B) = J_{c0}/(1+3|B|/B_K)$  with  $B_K = \mu_0 H_{c1}/3$  (Fig. 8) or  $B_K = \mu_0 a J_{c0}/3$  (Fig. 9). In Figs. 5, 7, and 9,  $H_{c1}$  is held constant; with increasing  $J_c$  or  $J_{c0}$  (in natural units  $H_{c1}/a$ ) the magnetization loops are inflated nearly symmetrically about the pin-free loop or about the reversible curve (above  $H_{rev}$ ), and the maximum of  $|M(H_a)|$  shifts to higher fields. Above  $H_{rev}$  the width of the loop is nearly proportional to  $J_c$ , as expected from theories [15,16] which assumed  $H_{c1} = 0$ , but

at small fields the influence of finite  $H_{c1}$  is clearly seen up to rather strong pinning.

In Figs. 6 and 8,  $J_c$  or  $J_{c0}$  is held constant and  $H_{c1}$  increased from zero (in natural units  $aJ_c$ ). As expected, the influence of finite  $H_{c1}$  is most pronounced at small applied fields  $H_a$ , where it causes a peak in  $-M$  even in the Bean magnetization curves, which without consideration of  $H_{c1}$  consist of two monotonic branches and a monotonic virgin curve. Within the Kim model, or with any decreasing  $J_c(B)$  dependence, the magnetization loops exhibit a maximum even when  $H_{c1} = 0$  is assumed [19]. With increasing  $H_{c1}$  this maximum becomes sharper and shifts to larger fields, cf. Fig. 8. Comparing Figs. 5 and 9 one sees that for superconductor disks with pinning and with  $H_{c1} > 0$ , the peak in  $-M(H_a)$  becomes more pronounced and shifts towards smaller applied fields when the disk thickness is decreased.

- [1] P. W. Anderson, Phys. Rev. Lett. **9** (1962) 309.
- [2] J. Provost, E. Paumier, and A. Fortini, J. Phys. F **4**, 439 (1974); A. Fortini, A. Haire, and E. Paumier, Phys. Rev. B **21** (1980) 5065.
- [3] C. P. Bean and J. D. Livingston, Phys. Rev. Lett. **12** (1964) 14; L. Burlachkov, Phys. Rev. B **47** (1993) 8056.
- [4] M. V. Indenbom, H. Kronmüller, T. W. Li, P. H. Kes, and A. A. Menovsky, Physica C **222** (1994) 203; M. V. Indenbom and E. H. Brandt, Phys. Rev. Lett. **73** (1994) 1731; E. H. Brandt, Rep. Prog. Phys. **58** (1995) 1465.
- [5] N. Morozov et al., Phys. Rev. Lett. **76** (1996) 138; N. Morozov et al., Physica C **291** (1997) 113;
- [6] E. Zeldov, A. I. Larkin, V. B. Geshkenbein, M. Konczykowski, D. Majer, B. Khaykovich, V. M. Vinokur, and H. Strikman, Phys. Rev. Lett. **73** (1994) 1428.
- [7] E. Zeldov et al., Physica C **235-240** (1994) 2761; B. Khaykovich et al., Physica C **235-240** (1994) 2757;
- [8] I. L. Maksimov and A. A. Elistratov, Pis'ma Zh. Eksp. Teor. Fiz. **61** (1995) 204 [Sov. Phys. JETP Lett. **61** (1995) 208]; I. L. Maksimov and A. A. Elistratov, Appl. Phys. Lett. **72** (1998) 1650.
- [9] Th. Schuster, M. V. Indenbom, H. Kuhn, E. H. Brandt, and M. Konczykowski, Phys. Rev. Lett. **73** (1994) 1424.
- [10] M. Benkraouda and J. R. Clem, Phys. Rev. B **53** (1996) 5716; Phys. Rev. B **58** (1998) 15103.
- [11] A. V. Kuznetsov, D. V. Eremenko, and V. N. Trofimov, Phys. Rev. B **56** (1997) 9064; Phys. Rev. B **57** (1998) 5412.
- [12] L. D. Landau and E. M. Lifshitz, *Electrodynamics of Continuous Media*, Vol. 8 of Course in Theoretical Physics (Pergamon Press, London, 1959).
- [13] G. P. Mikitik and E. H. Brandt, Phys. Rev. B **60** (1999) 592.
- [14] E. H. Brandt, Phys. Rev. Lett. **78** (1997) 2208.
- [15] E. H. Brandt, Phys. Rev. B **54** (1996) 4246.
- [16] E. H. Brandt, Phys. Rev. B **58** (1998) 6506, 6523.
- [17] R. Labusch and T. B. Doyle, Physica C **290** (1997) 143; T. B. Doyle, R. Labusch, and R. A. Doyle, Physica C **290** (1997) 148.
- [18] E. H. Brandt, Phys. Rev. B **59** (1999) 3369; **60** (1999) 11939.
- [19] D. V. Shantsev et al., Phys. Rev. Lett. **82** (1999) 2947.